

# Research on an Inverter-fed Six-Pole Permanent Magnet Biased Magnetic Bearing

Ji Li  
Nanjing University of  
Aeronautics and Astronautics  
Nanjing, China

Xu Longxiang  
Nanjing University of  
Aeronautics and Astronautics  
Nanjing, China

## Abstract

The configuration and working principle of a six-pole heteropolar permanent magnet biased magnetic bearing is introduced. And the mathematical models of the suspension forces are deduced through coordinate transformation. Then the paper studies the performances of the magnetic bearing for various area ratios between the permanent magnetic pole and the electromagnetic pole. The mathematical models are verified by finite element simulation. The results show that the current stiffness error rate between theoretical calculation and finite-element simulation is less than 3%, while the displacement stiffness error rate is much greater. A controller for this magnetic bearing is designed. To confirm the controller is effective, experiments were carried out with the proposed magnetic bearing system. The results all show that the rotor can be suspended steadily and the whole control system has good dynamic and static performance with robustness. Finally, power losses tests were done. As a result, the power losses of proposed six-pole magnetic bearing are only 9.85% of the traditional eight-pole active magnetic bearing for the same bias magnetic flux density.

## 1 Introduction

As the utilization of rare earth permanent magnet, permanent magnet biased magnetic bearing has characteristics of small size, high efficiency and low running cost. For these advantages it has been widely used in the areas of energy storage flywheel, wind power generation, high speed blower and compressor, etc. [1-4].

Previous researches of permanent magnet biased magnetic bearing focused on homo-polar ones [5]. This type of magnetic bearing has uncomplex mechanical construction and can reduce hysteresis loss of rotor so it is widely used in many industries [6-7]. However, such magnetic bearing increases axial length in order to project a closed loop for bias flux, which restricts the improvement of critical speed of rotor system. Moreover, as the exiting of an axial crossing of bias flux the leakage coefficient of this magnetic bearing is much larger than traditional eight-pole active magnetic bearing [8]. Newer evolutions strive for the commitment of hetero-polar type that has both advantages of low leakage coefficient and low running cost without excess axial length. Nowadays, the most common configuration of hetero-polar permanent magnet biased magnetic bearing is an eight-pole one which was presented by scholar Yohji Okada in the ninth International Symposium on Magnetic Bearings [9]. Further investigations also have been done in the literature [10-11]. Recently, scholar Martin Reisinger proposed a novel design of six-pole hetero-polar permanent magnet biased magnetic bearing which can be practiced with traditional three-phase voltage source inverters [12]. This paper investigates the configuration, functionality, control method and running cost of this six-pole magnetic bearing.

## 2 Model of the six-pole magnetic bearing

### 2.1 Functionality of the six-pole magnetic bearing

The arrangement of proposed magnetic bearing is showed in fig.1. Such magnetic bearing consists of an iron ring with three permanent magnet poles and three iron poles. The permanent magnet poles marked a, b, c are used to generate bias flux by each of the permanent magnets. The iron poles marked 1, 2, 3 are wounded by magnetic coils to produce control flux dependent on the three phase magnetic motive force. The dashed lines in figure 1 indicate

---

\*E-mail: [jiliglittering@nuaa.edu.cn](mailto:jiliglittering@nuaa.edu.cn), Address: No.29 Yudao St. Nanjing China, Phone Number: +86-025-84892594

the bias flux and the control flux is indicated by the solid lines. In this paper, the direction of flux is from permanent magnet poles to iron poles. As a result, for control magnetic motive force, the positive direction is to enhance this trend.

When the rotor is in the equilibrium position, flux densities generated by permanent magnets in all air gaps are equal due to the symmetry of structure symmetry, which means there are no magnetic force between stator and rotor in both x and y direction. When a force in the negative y-direction is generated, the rotor position will create an error from equilibrium position along negative y-direction. Then the controller will generate a magnetic motive force in the positive y-direction based on the error detected by position sensor. This magnetic motive force will increase the flux density in the air gap between iron pole 1 and rotor whereas the magnetic flux densities in the air gaps of the iron pole 2 and 3 are accordingly decreased. As a result, a magnetic force in the rotor along positive y-direction is created to drag rotor back to the equilibrium position.

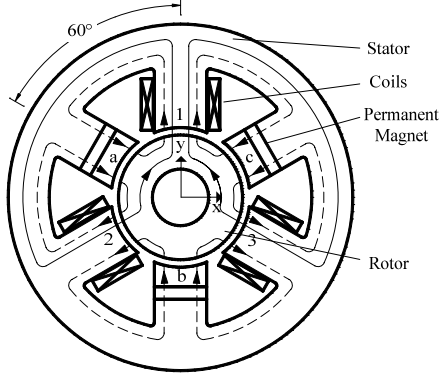


Figure 1: Arrangement principle of six-pole permanent magnet biased magnetic bearing

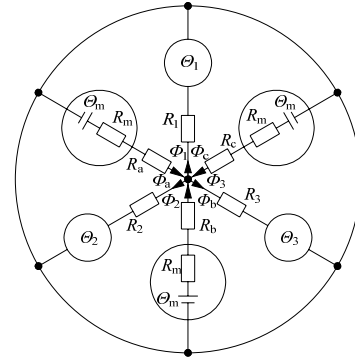


Figure 2: Equivalent magnetic circuit for the proposed magnetic bearing

## 2.2 Mathematical models of the suspension forces

The equivalent magnetic circuit is given in fig.2. Where,  $\Theta_1$ ,  $\Theta_2$ ,  $\Theta_3$  and  $\Theta_m$  are the electromagnetic motive force created by coils 1, 2, 3 and permanent magnet respectively.  $R_i$  and  $\Phi_i$  which ( $i=1, 2, 3, a, b, c$ ) indicate the reluctance and magnetic flux separately for the corresponding air gaps.  $R_m$  expresses the reluctance for permanent magnet.

The magnetic force is calculated based on ampere's loop law ignoring magnetic saturation and assuming that the reluctances exist only in the air gaps.

For bias flux, the magnetic field lines generated by permanent magnet are from permanent magnet pole a to rotor crossing the air gaps, then closed over the pole 1, 2. The flux in air gap 1 is created by permanent magnet a and c. At the same time, permanent magnet a and b work together to generate the magnetic flux in the air gap 2. Then the equations of bias flux can be obtained as (1) to (4).

$$\Theta_m = \Phi_a R_a + \Phi_a \left( \frac{R_1 R_2}{R_1 + R_2} \right) \quad (1)$$

$$\Phi_a = \frac{\Theta_m (R_1 + R_2)}{R_1 R_a + R_2 R_a + R_1 R_2} \quad (2)$$

$$\Phi_{a1} = \frac{\Theta_m R_2}{R_1 R_a + R_2 R_a + R_1 R_2} \quad (3)$$

$$\Phi_{a2} = \frac{\Theta_m R_1}{R_1 R_a + R_2 R_a + R_1 R_2} \quad (4)$$

In the equations above,  $\Phi_a$ ,  $\Phi_{a1}$ ,  $\Phi_{a2}$  indicate the magnetic flux in the air gap a, 1 and 2 that created by permanent magnet a.

Reluctances in the air gaps can be expressed as

$$R_i = \frac{\delta_i}{\mu_0 S_i} \quad (5)$$

Here,  $\mu_0$  is permeability of vacuum,  $S_i$  and  $\delta_i$  are the pole area and air gap length in the air gap  $i$ . Substituting (5) into (2), (3), (4), the bias flux generated by permanent magnet a can be described as follows

$$\begin{cases} \Phi_a = \mu_0 S \frac{\Theta_m (\delta_1 + \delta_2)}{\delta_1 \delta_a + \delta_2 \delta_a + \delta_1 \delta_2} \\ \Phi_{a1} = \mu_0 S \frac{\Theta_m \delta_2}{\delta_1 \delta_a + \delta_2 \delta_a + \delta_1 \delta_2} \\ \Phi_{a2} = \mu_0 S \frac{\Theta_m \delta_1}{\delta_1 \delta_a + \delta_2 \delta_a + \delta_1 \delta_2} \end{cases} \quad (6)$$

The bias flux generated by permanent magnet b and c can be described as

$$\begin{cases} \Phi_b = \mu_0 S \frac{\Theta_m (\delta_2 + \delta_3)}{\delta_2 \delta_b + \delta_3 \delta_b + \delta_2 \delta_3} \\ \Phi_{b2} = \mu_0 S \frac{\Theta_m \delta_3}{\delta_2 \delta_b + \delta_3 \delta_b + \delta_2 \delta_3} \\ \Phi_{b3} = \mu_0 S \frac{\Theta_m \delta_2}{\delta_2 \delta_b + \delta_3 \delta_b + \delta_2 \delta_3} \end{cases} \quad (7)$$

$$\begin{cases} \Phi_c = \mu_0 S \frac{\Theta_m (\delta_3 + \delta_1)}{\delta_3 \delta_c + \delta_1 \delta_c + \delta_3 \delta_1} \\ \Phi_{c3} = \mu_0 S \frac{\Theta_m \delta_1}{\delta_3 \delta_c + \delta_1 \delta_c + \delta_3 \delta_1} \\ \Phi_{c1} = \mu_0 S \frac{\Theta_m \delta_3}{\delta_3 \delta_c + \delta_1 \delta_c + \delta_3 \delta_1} \end{cases} \quad (8)$$

The control flux created by electromagnetic motive force almost can not circulating through three permanent magnet poles considering the reluctance of permanent magnets, they close over three iron poles and the keeper as shown in fig.1. As a result, the formulation of equivalent magnetic circuit is the same as a traditional three-pole AC magnetic bearing. So the control flux in the air gaps 1, 2 and 3 can be expressed as

$$\begin{cases} \Phi_{d1} = \mu_0 S \frac{(\delta_2 + \delta_3)\Theta_1 - \delta_3\Theta_2 - \delta_2\Theta_3}{\delta_1\delta_2 + \delta_2\delta_3 + \delta_3\delta_1} \\ \Phi_{d2} = \mu_0 S \frac{(\delta_3 + \delta_1)\Theta_2 - \delta_3\Theta_1 - \delta_1\Theta_3}{\delta_1\delta_2 + \delta_2\delta_3 + \delta_3\delta_1} \\ \Phi_{d3} = \mu_0 S \frac{(\delta_1 + \delta_2)\Theta_3 - \delta_2\Theta_1 - \delta_1\Theta_2}{\delta_1\delta_2 + \delta_2\delta_3 + \delta_3\delta_1} \end{cases} \quad (9)$$

Based on (6), (7), (8) and (9), the magnetic flux in the air gap 1, 2 and 3 can be calculated as

$$\begin{cases} \Phi_1 = \Phi_{d1} + \Phi_{a1} + \Phi_{c1} \\ \Phi_2 = \Phi_{d2} + \Phi_{a2} + \Phi_{b2} \\ \Phi_3 = \Phi_{d3} + \Phi_{b3} + \Phi_{c3} \end{cases} \quad (10)$$

If the rotor in the x- and y-direction has small positive displacement  $x$  and  $y$ , the air gap width  $\delta_i$  can be expressed as

$$\begin{bmatrix} \delta_1 \\ \delta_2 \\ \delta_3 \\ \delta_a \\ \delta_b \\ \delta_c \end{bmatrix} = \begin{bmatrix} 1 & 0 & -1 \\ 1 & \frac{\sqrt{3}}{2} & \frac{1}{2} \\ 1 & -\frac{\sqrt{3}}{2} & \frac{1}{2} \\ 1 & \frac{\sqrt{3}}{2} & -\frac{1}{2} \\ 1 & 0 & 1 \\ 1 & -\frac{\sqrt{3}}{2} & -\frac{1}{2} \end{bmatrix} \begin{bmatrix} \delta_0 \\ x \\ y \end{bmatrix} \quad (11)$$

Considering the coordinate transformation of 3s/2s

$$\begin{bmatrix} i_1 \\ i_2 \\ i_3 \end{bmatrix} = \sqrt{\frac{2}{3}} \begin{bmatrix} 0 & 1 \\ -\frac{\sqrt{3}}{2} & -\frac{1}{2} \\ \frac{\sqrt{3}}{2} & -\frac{1}{2} \end{bmatrix} \begin{bmatrix} i_x \\ i_y \end{bmatrix} \quad (12)$$

Where  $i_1, i_2, i_3$  are the current in the coils 1, 2, 3;  $i_x, i_y$  are the x- and y-direction components of the excitation current. The relationship between current and electromagnetic motive force is given by

$$\begin{cases} \Theta_1 = N \cdot i_1 \\ \Theta_2 = N \cdot i_2 \\ \Theta_3 = N \cdot i_3 \\ \Theta_m = N \cdot i_m \end{cases} \quad (13)$$

Here,  $N$  is the turns of coils and  $i_m$  is the equivalent excitation current of permanent magnets. So the magnetic suspension forces in x-and y-direction can be calculated as follows

$$\begin{cases} F_x = \frac{\sqrt{3}}{4\mu_0 S} (\Phi_3^2 - \Phi_2^2 + \Phi_c^2 - \Phi_a^2) \\ F_y = \frac{1}{4\mu_0 S} (2\Phi_1^2 - \Phi_2^2 - \Phi_3^2 - 2\Phi_b^2 + \Phi_a^2 + \Phi_c^2) \end{cases} \quad (14)$$

Substituting (10), (11), (12) and (13) into (14), under the assumption that the rotor has a very small displacement from the radial balanceable position, (14) can be linearized as follows

$$\begin{cases} F_x = F_x \Big|_{\substack{i_x=i_y=0 \\ x=y=0}} + \frac{\partial F_x}{\partial x} \Big|_{\substack{i_x=i_y=0 \\ x=y=0}} \cdot x + \frac{\partial F_x}{\partial y} \Big|_{\substack{i_x=i_y=0 \\ x=y=0}} \cdot y + \frac{\partial F_x}{\partial i_x} \Big|_{\substack{i_x=i_y=0 \\ x=y=0}} \cdot i_x + \frac{\partial F_x}{\partial i_y} \Big|_{\substack{i_x=i_y=0 \\ x=y=0}} \cdot i_y \\ F_y = F_y \Big|_{\substack{i_x=i_y=0 \\ x=y=0}} + \frac{\partial F_y}{\partial x} \Big|_{\substack{i_x=i_y=0 \\ x=y=0}} \cdot x + \frac{\partial F_y}{\partial y} \Big|_{\substack{i_x=i_y=0 \\ x=y=0}} \cdot y + \frac{\partial F_y}{\partial i_x} \Big|_{\substack{i_x=i_y=0 \\ x=y=0}} \cdot i_x + \frac{\partial F_y}{\partial i_y} \Big|_{\substack{i_x=i_y=0 \\ x=y=0}} \cdot i_y \end{cases} \quad (15)$$

The linear equation of magnetic suspension forces can be written as

$$\begin{cases} F_x = k_{xy} x + k_1 i_x \\ F_y = k_{xy} y + k_1 i_y \end{cases} \quad (16)$$

Where displacement stiffness  $k_{xy} = 1.3333 \mu_0 SN^2 i_m^2 / \delta_0^3$ , current stiffness  $k_i = 0.8165 \mu_0 SN^2 i_m / \delta_0^2$ . Comparing with traditional eight-pole active magnetic bearing ( $k_{xy} = 0.8536 \mu_0 SN^2 i_0^2 / \delta_0^3$ ,  $k_i = 0.9239 \mu_0 SN^2 i_0 / \delta_0^2$ ), the displacement stiffness of this proposed magnetic bearing is larger, while the current stiffness is smaller in the case of  $i_m = i_0$ . On the other hand, the control algorithm for the proposed magnetic bearing is much simpler than traditional three-pole AC magnetic bearing for the utilization of two independent controllers as the decoupling in x-and y-direction.

As the utilization of passive suspension in the three permanent magnet poles the displacement stiffness of the proposed bearing is larger. It is a disadvantage for the stability of the control system. But it can be overcome by reducing the area of permanent magnet poles. Assume that the areas of three iron poles are  $S$ , and three permanent magnet poles are  $\lambda S$ , where  $\lambda$  is area coefficient with the range of zero to one. Then the expression of displacement stiffness and current stiffness can be rewritten as:  $k_{xy} = \lambda_{xy} \mu_0 SN^2 i_m^2 / \delta_0^3$ ,  $k_i = \lambda_i \mu_0 SN^2 i_m / \delta_0^2$ . Where,  $\lambda_{xy}$  and  $\lambda_i$  are the influence coefficient based on the area coefficient  $\lambda$ . The characteristic curves regarding  $\lambda$  are illustrated in fig.3.

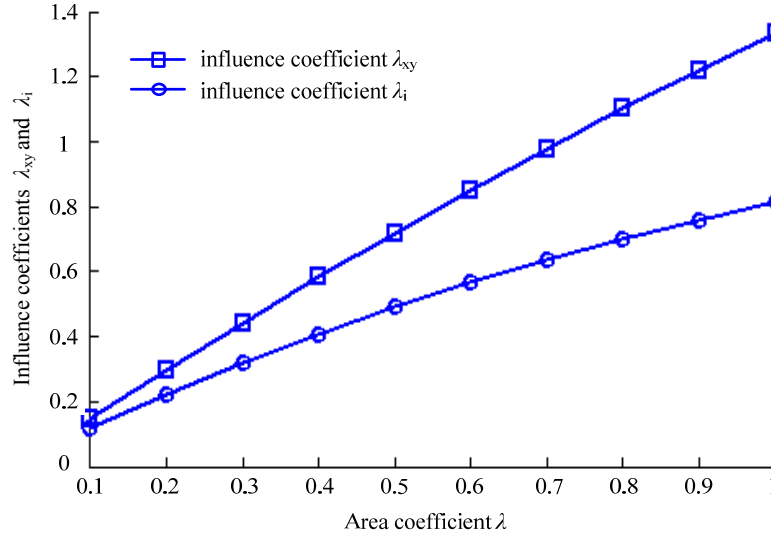


Figure 3: Influence coefficient  $\lambda_{xy}$  and  $\lambda_i$  for various  $\lambda$

### 3 Finite element analysis

In this section, simulations for the proposed magnetic bearing are carried out using 2D finite element program to verify the previous analysis. The utilized simulation quantities are shown in table 1.

Dimension and property	Specification
Air gap in radial, $\delta_0$ (mm)	0.25
Inner diameter of stator, $d_i$ (mm)	40.3
Outer diameter of stator, $d_e$ (mm)	105
Axial length of stator, $L$ (mm)	25
Thickness of stator yoke, $h_j$ (mm)	12.5
Tooth width of stator $b$ (mm)	10
Area of permanent magnet $A_m$ (mm <sup>2</sup> )	225
Thickness of permanent magnet $h_m$ (mm)	5
Area coefficient $\lambda$	1
Turns of control coils $N$	100

Table 1: Parameters of the model

The simulation results for bias flux shown in fig.4 and 5. Fig.4 shows the distribution of magnetic flux density when the rotor is located in the equilibrium position without any electrical exciting. The result points out the bias flux generated by three permanent magnets distribute uniformly in the stator and rotor, the magnetic flux density in all six air gaps is equal with 0.81T as shown in fig.5.

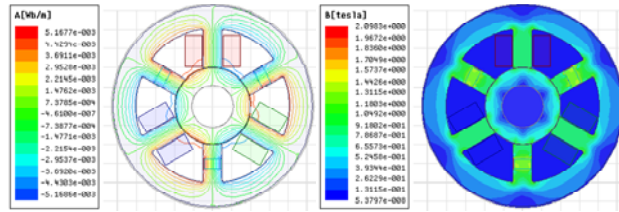


Figure 4: distribution of bias flux density

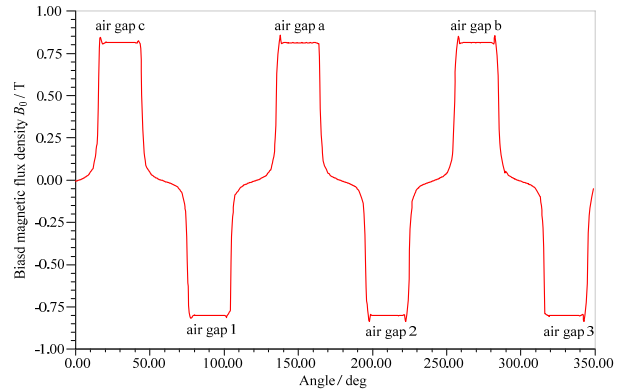


Figure 5: Distribution of bias flux density in each air gap

The comparing results of suspension forces for various exciting current between calculation and simulation with the rotor in the equilibrium position are shown in fig. 6a and 6b. As a result, it has satisfying linearity between the suspension forces and exciting current nearby the operating point. The component of current in x-direction can affect suspension force in y-direction slightly in nonlinear area, whereas y-direction current only contribute to the y-direction suspension force. From the comparison, we can obtain that in the x- and positive y-direction the results between calculation and simulation are very close with the error rate of 2.63% and 2.62%, while the error is much larger in negative y-direction when the exciting current  $i_y$  below -1A.

Figures 6c and 6d indicate the suspension force acting on the rotor as a function of the rotor displacement in relation to the centre without any exciting current. We can obtain the linearity of the characteristic curves by simulation is better in the x-direction than y-direction with the displacement from -0.1mm to 0.1mm. As the asymmetry of configuration in y-direction, the displacement in x-direction will generate magnetic force acting on the rotor along y-axis, whereas there is no coupling identity between y-direction displacement and x-direction suspension force. Comparing the results by calculation and simulation, the average error rate of displacement stiffness is considerable with 60.97% in x-direction and 22.58% in y-direction. That is because the rotor has been seen as a particle which is less accurate for calculating the relative displacement from each pole in the formulating of equivalent magnetic circuit. So that the displacement stiffness obtained by the solution of equivalent magnetic circuit should be revised by finite element analyses or experiment.

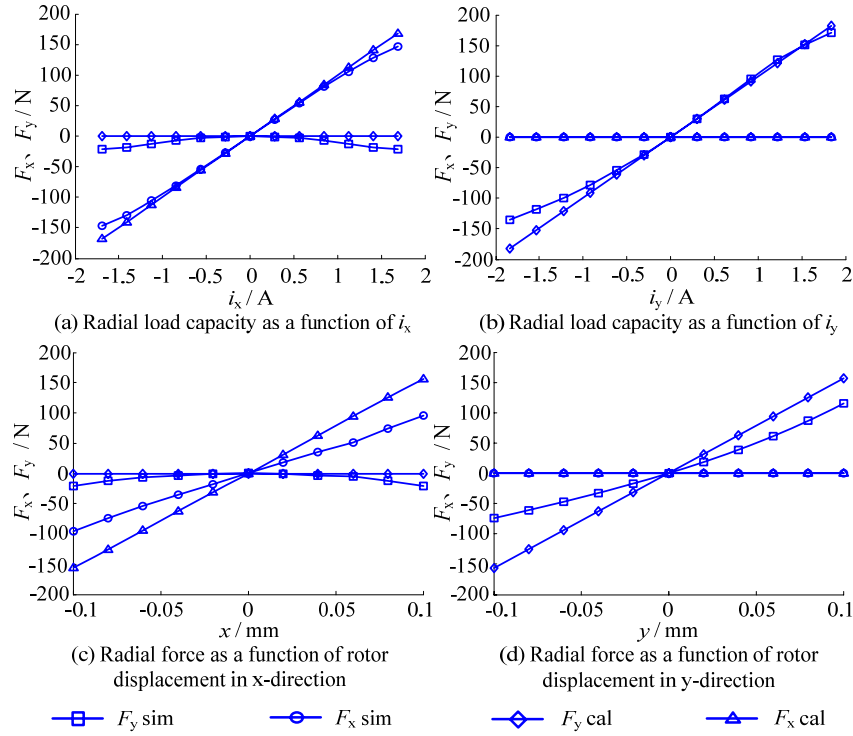


Figure 6: Comparing results of suspension forces between calculation and simulation

## 4 Design and simulation for control system

Although the linear model of suspension force is less accurate with the deviation from the operating point, it is still reliable for the design of controller as the experimental verification. So that according to Newton's second law and Laplace transform, the transfer function from exciting current to displacement of rotor can be expressed as

$$G(s) = \frac{k_i}{ms^2 - k_{xy}} \quad (17)$$

Where  $m$  is the mass of rotor.

For (17), the feedback system can be projected as Fig. 7, where the block  $k_A$  and  $k_S$  are gains of inverter and position sensor. As the decoupling in the solution of suspension force, the traditional PID controller can be used and its transfer function is as follows

$$G_C(s) = k_p \left( 1 + \frac{1}{\tau_i s} + \tau_d s \right) \quad (18)$$

Here,  $k_p$  is proportional coefficient,  $\tau_i$  is Integral coefficient and  $\tau_d$  is differential coefficient.

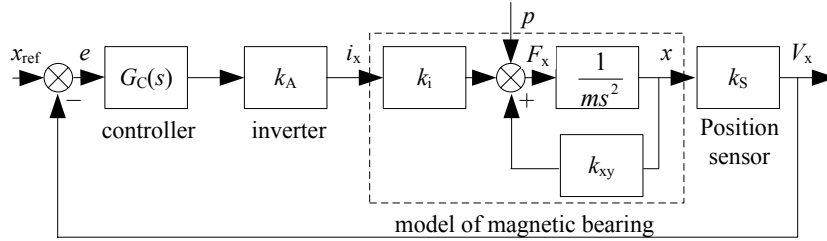


Figure 7: Control system of magnetic bearing

### 4.1 Simulation results

For verification, a simulation will be presented based on nonlinear mathematical model in Matlab/Simulink. The block diagram of position loop control system is shown as

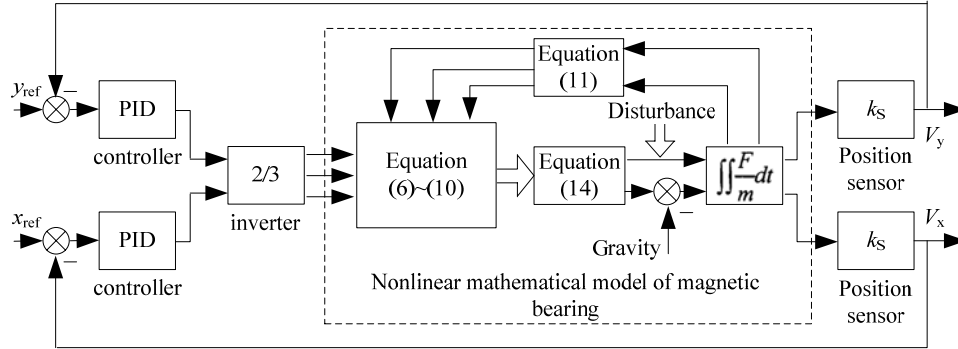


Figure 8: Control structure of the proposed magnetic bearing

Fig.9a and 9b show the transient response of exciting current and rotor displacement in the 0.03s after levitation control action. Where  $i_y$  raise to about 0.12A in 0.3ms to compensate the gravity acted on the rotor, whereas  $i_x$  keeps constant. Overcome the influence of gravity, rotor return to equilibrium position in about 5ms. At the simulation time 40ms, a disturbing force has been imposed to the rotor with 50N and 10ms action time, and the simulation waveforms are shown in fig.9c and 9d. In order to overcome this disturbing force, both  $i_x$  and  $i_y$  increase in positive direction then return to previous states with the regression of the disturbing force, which is about 20ms in the whole process. And the vibration of rotor is less than  $\pm 2\mu\text{m}$ .

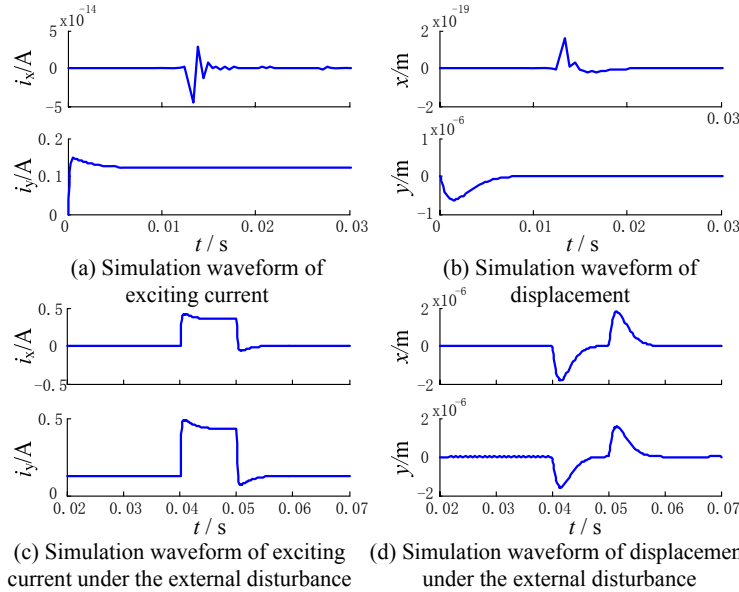


Figure 9: Simulation results for control system in Matlab/Simulink

## 5 Experiment results

In this section, experiments will be carried out to verify the previous analysis. The experiments have been done with a digital controller based on TMS320F28335 on a prototype six-pole magnet biased magnetic bearing system as shown in fig.10. The following figures are draw by the data captured by digital oscilloscope WaveRunner 64Xi-A. Eddy current sensors are used in the experiments for the detection of the rotor position with the sensitivity of 32V/mm, measurement range of -4V~4V.

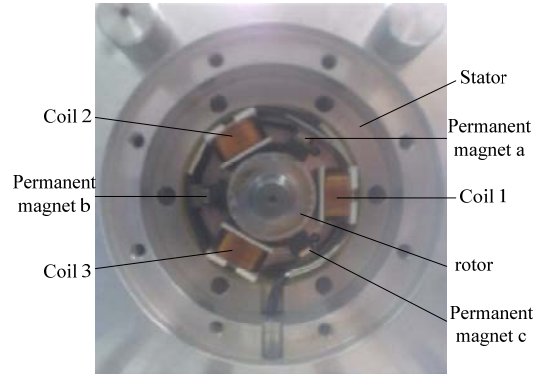


Figure 10: Functional prototypes of proposed magnetic bearing

## 5.1 Suspension tests

Fig.11 shows the response of displacement and current after levitation suspension action. From fig.11a and 11b, the initial position of rotor is  $x=-0.071875\text{mm}$ ,  $y=-0.09375\text{mm}$ . By the activation of proposed magnetic bearing the rotor can be suspended stably within 50ms. The transient responses of control current in three phase windings are showed in fig.11c. The steady-state residual current of  $i_1$ ,  $i_2$ ,  $i_3$  are about 0A, 0.3A, -0.3A. That is because the horizontal of y-direction, as shown in fig.10. In that case, the gravity of rotor is bear by x-direction. As a result, the controller has to increase the magnetic flux density in air gap 2, while decrease the magnetic flux density in air gap 3, to compensate the gravity of rotor. In the process, the axis orbit of rotor is shown in fig.11d.

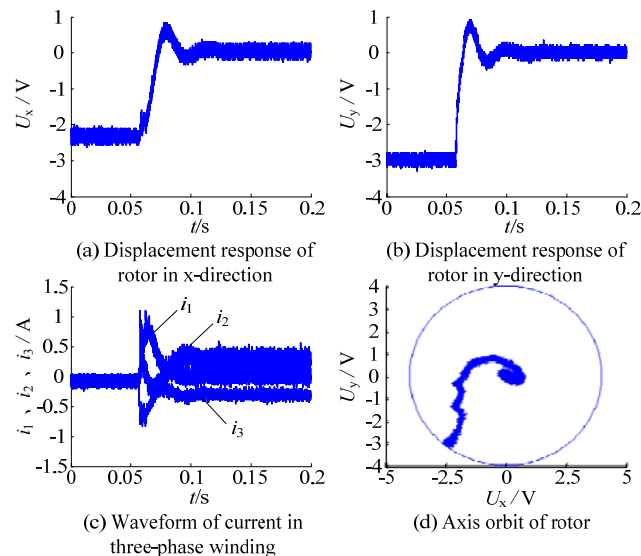


Figure 11: Response of displacement and current after levitation suspension action

The speed-up tests have been done in a five freedom magnetic bearing test-bed. As shown in fig.12, the test-bed consists of a rotor, a traditional eight-pole radial active magnetic bearing, an axial active magnetic bearing, a high-speed motor and a proposed six-pole magnetic bearing. The mass and moment of inertia of the rotor are 2.2kg and  $3.8 \times 10^2 \text{kgmm}^2$ .



Figure 12: Five freedom magnetic bearing test-bed

For the steady-state, the displacement signal waveform of  $x$ ,  $y$  directions are shown in fig.13a and 13b. The residual displacement signal remained less than 288mV, for the actual displacement of  $4.5\mu\text{m}$ . In a speed-up test, the rotor could successfully rotate up to 13800r/min, with the displacement of  $6.5\mu\text{m}$  and  $7\mu\text{m}$  separately in  $x$  and  $y$  direction.

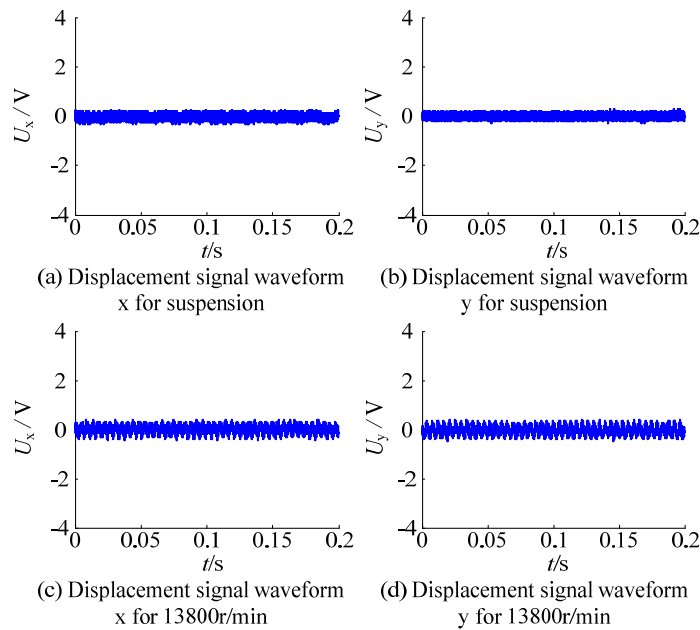


Figure 13: Displacement signal waveform for steady-state and 13800r/min

## 5.2 Dynamic Response tests

In the steady-state, an impact force has been applied to the rotor in positive  $x$ -direction at the time 0.1s. The displacement responses of  $x$  and  $y$  are shown in fig.14a, 14b. The disturbing force engenders a vibration on the rotor in positive  $x$ -direction of  $90\mu\text{m}$ . After about 50ms the rotor goes back to equilibrium position. Although there is no external force acted on  $y$ -direction, the displacement signal  $U_y$  still appears a fluctuation about  $50\mu\text{m}$ . Whereas, the displacement  $x$  almost has no effect with the impact in  $y$ -direction from fig.14c, 14d. From the test results, we can obtain that the whole control system has good dynamic performance. And they verify the simulation conclusion in section 2 that the displacement in  $x$ -direction will generate magnetic force acting on the rotor along  $y$ -axis, whereas there is no coupling identity between  $y$ -direction displacement and  $x$ -direction suspension force.

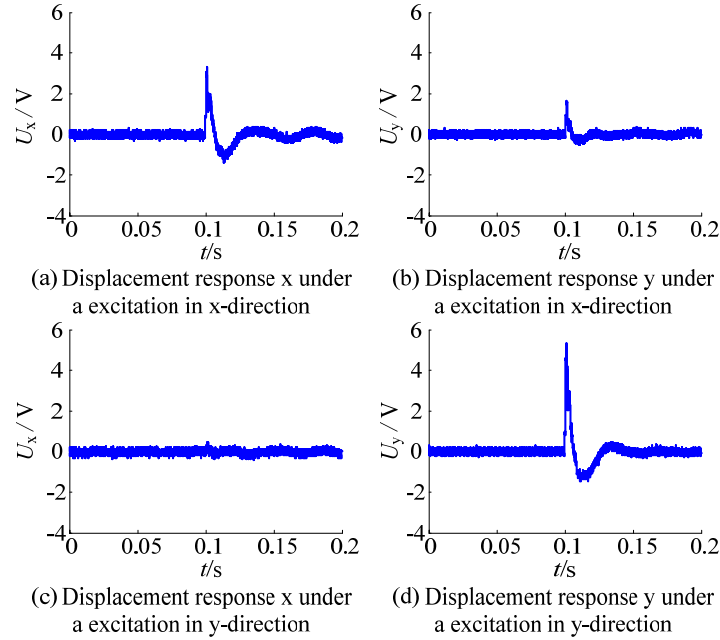


Figure 14: Displacement response of x and y under an impact force

### 5.3 Power losses tests

For a active magnetic bearing system, the running cost mainly includes copper loss by control windings, iron loss by ferromagnetic material and switching loss by power amplifier. In this test, a three-phase power analyzer WT1800 was used to measure the input and output power of power amplifier synchronously, so that the switching loss ( $P_S$ ) and the sum of copper loss and iron loss ( $P_{CU+FE}$ ) could be separated from total power losses ( $P_{ALL}$ ). In the test, firstly, make proposed six-pole magnetic bearing work stably for one hour. After temperature condition is satisfied, record data every 2 minutes. The losses curves can be obtained as fig.15a. The average of  $P_{ALL}$ ,  $P_S$ ,  $P_{CU+FE}$  is respectively 12.77W, 5.03W and 7.74W. Raise the rotational speed of rotor from 0 to 13800r/min, record the losses every 600r/min. The losses curves are shown as fig.15b. Note that, as the increasing of speed,  $P_{ALL}$  and  $P_{CU+FE}$  encounter a fluctuation, but there is no obvious up or down trend both in  $P_{ALL}$ ,  $P_S$  and  $P_{CU+FE}$ . As a result, a conclusion can be made as the power losses of proposed magnetic bearing itself are independent with the speed of rotor within 13800r/min.

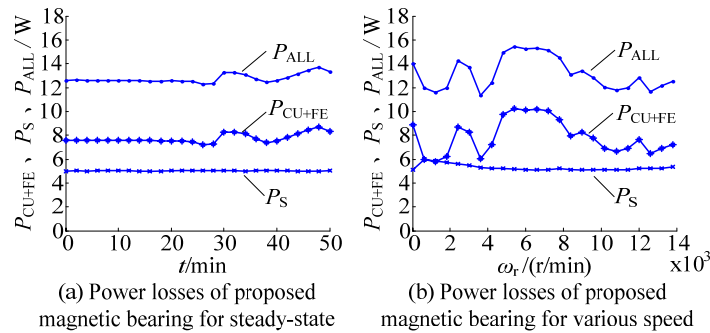


Figure 15: Power losses curves for the proposed six-pole magnetic bearing

A comparative test has been done for the traditional eight-pole active magnetic bearing with the same size in the five-freedom test-bed. According to the comparability in  $P_S$ , the same power devices and driving Circuit have been used. Fig.16a shows the losses curves for the eight-pole active magnetic bearing with the same bias magnetic flux density to the proposed six-pole magnetic bearing of 0.8T. As shown in fig.16a, the average of  $P_{ALL}$ ,  $P_S$ ,  $P_{CU+FE}$  is respectively 129.69W, 112.69W and 19W. In contrast with the former test, the proposed six-pole magnetic bearing has lower power losses with the percentage of  $P_{ALL}$  9.85%,  $P_S$  4.46% and  $P_{CU+FE}$  40.74%. As the different surface

area of magnetic poles, the bearing capacity of eight-pole active magnetic bearing is larger than proposed six-pole magnetic bearing with the same bias magnetic flux density. By turning down the bias current, the power loss components are also plotted in the similar manner for the eight-pole active magnetic bearing when the bias magnetic flux density  $B_0=0.6\text{T}$ , as shown in fig.16b. This figure shows that the  $P_{ALL}$ ,  $P_S$  and  $P_{CU+FE}$  are both decreased with the average of 95.62W, 85.32W and 10.3W. In that case, the percentage of power losses between proposed six-pole magnetic bearing and eight-pole active magnetic bearing is respectively  $P_{ALL}$  13.35%,  $P_S$  5.90% and  $P_{CU+FE}$  75.15%. Comparing with traditional eight-pole active magnetic bearing, the proposed six-pole magnetic bearing showed significantly lower power losses, especially in the switching loss.

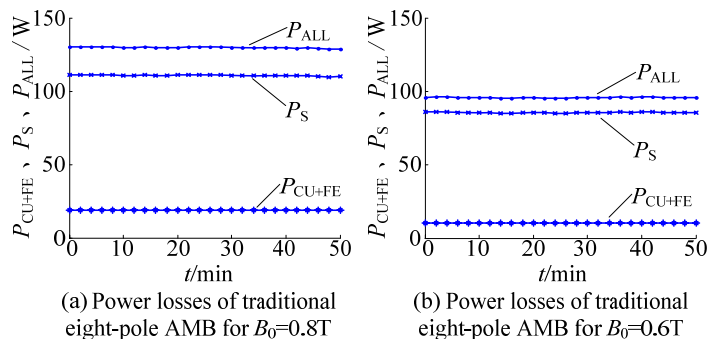


Figure 16: Power losses curves for traditional eight-pole active magnetic bearing

In order to measure the power losses that caused by rotation, the run down tests were performed on the five-freedom test-bed with above two bearings for the speed of 12000r/min. Fig.17a shows a typical set of three run down plots for the proposed six-pole magnetic bearing for curve 2 and eight-pole active magnetic bearing of  $B_0=0.6\text{T}$  and  $0.8\text{T}$  respectively for curve 1 and curve 3. For this figure, when above the rotational speed of 7000r/min, curve 2 and 3 decrease more sharply than curve 1. However, with the continual decline of speed, the downtrend of curve 2 turns slow gradually. Finally, curve 1 and 2 decreased to zero at nearly the same time, whereas the dropping time of curve 3 is shorter.

An extra power loss ( $P_E$ ) was determined by the method described in [13]. A plot of the extra power loss in Watts versus rotor speed for the above two bearings are shown in fig.17b, where curve 5 for the proposed six-pole magnetic bearing, curve 6 and 4 for eight-pole active magnetic bearing of  $B_0=0.6\text{T}$  and  $0.8\text{T}$  respectively. The extra loss is the total power loss including electromagnetic power loss from magnetic bearings and windage losses along the entire length of the rotor. As shown in fig.17b,  $P_E$  for the three rundown cases is respectively 15.8W, 13.9W and 15.4W when the speed of 12000r/min. for the higher speed,  $P_E$  for curve 5 is similar to curve 4, and higher than curve 6. Along with the decline of speed,  $P_E$  for curve 5 approaches which for curve 6 gradually. Whereas  $P_E$  for curve 4 still higher than those two. As the utilization of a same rotor in the tests, the windage losses are constant. We can obtain that  $P_E$  for the proposed six-pole magnetic bearing is very close to the traditional eight-pole active magnetic bearing with the same  $B_0$  at high rotational speed, but with the decline of speed,  $P_E$  for the proposed bearing drop more obviously.

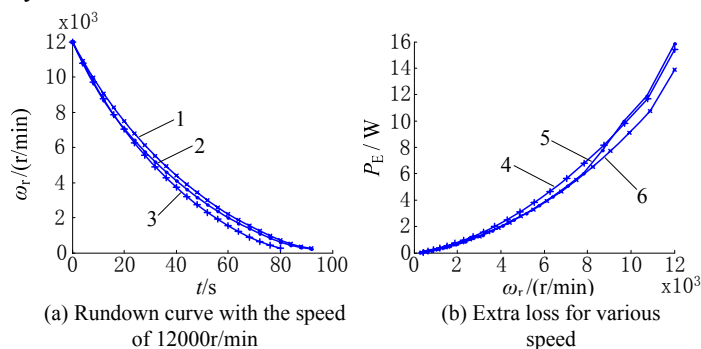


Figure 17: results for run down tests

## 6 Conclusion

This paper study a six-pole permanent magnet biased magnetic bearing. According to theory analysis and verification experiments it can obtain conclusion as

The displacement stiffness and the current stiffness of the proposed magnetic bearing both fall along with the decline of area coefficient  $\lambda$  while the downtrend of displacement stiffness is more sharply.

Compared with traditional eight-pole active magnetic bearing the displacement stiffness of this proposed magnetic bearing is larger, while the current stiffness is smaller in the case of  $\lambda=1$ .

The control algorithm for the proposed magnetic bearing is much simpler than traditional three-pole AC magnetic bearing for the utilization of two independent controllers to decouple in x-and y-direction.

As the results of 2D finite element analysis, the linearity between the suspension forces and exciting current in x-direction is better than y-direction and the calculation of current stiffness is closer to the finite element simulation than displacement stiffness.

The finite element analysis and experiments show that the displacement in x-direction will generate magnetic force acting on the rotor along y-axis, whereas there is no coupling identity between y-direction displacement and x-direction suspension force.

The simulations and experiments show that the rotor can be suspended steadily and the whole control system has good dynamic and static performance as well as good robustness.

From the results of Power losses tests, the power losses of proposed magnetic bearing itself are independent with the speed of rotor within 13800r/min.

For the results of experiments, comparing with traditional eight-pole active magnetic bearing, the proposed six-pole magnetic bearing showed significantly lower power loss, especially in the switching loss.

As the results of run down tests, the extra loss for the proposed six-pole magnetic bearing is very close to the traditional eight-pole active magnetic bearing with the same  $B_0$  at high rotational speed, but with the decline of speed, the extra loss for the proposed bearing drop more obviously.

## References

- [1] Schweiter G., Bleuler H., Traxler A. *Active Magnetic Bearings—Basics, Properties and Application of Active Magnetic Bearings*. Academic Press, Switzerland, 1994.
- [2] Sun Jinji, Fang Jiancheng. A novel structure of permanent magnet biased radial hybrid magnetic bearing. *Journal of Magnetism and Magnetic Materials*, 323(2), 2011.
- [3] Brian T. Murphy, Hamid Ouroua, Matthew T. Caprio, et al. Permanent magnet bias. homopolar magnetic bearings for a 130kW-hr composite flywheel. In *9th International Symposium on Magnetic Bearings*, August 2004.
- [4] Christian Ehmman, Tilo Sielaff, Rainer Nordmann. Comparison of active magnetic bearings with and without permanent magnet bias. In *9th International Symposium on Magnetic Bearings*, August 2004.
- [5] Zhao Xusheng, Deng Zhiqiu, Wang Xiaolin, et al. Research Status and Development of Permanent Magnet Biased Magnetic Bearings. *Transactions of China Electrotechnical Society*, 24(9), 2009.
- [6] Zhilichev Y. Analysis of a magnetic bearing pair with a permanent magnet excitation. *IEEE Transactions on Magnetics*, 36(5), 2000.
- [7] Zeng Li, Wang Tongyue, Xu Longxiang, et al. Study on mechanism for PMEB to produce magnetic suspension force. *Acta Aeronautica Et Astronautica Sinica*, 21(3), 2000.
- [8] Sun Jinji, Fang Jiancheng, Wang Xi, et al. A New Permanent Magnet Biased Radial Magnetic Bearing. *Transactions of China Electrotechnical Society*, 24(11), 2009.
- [9] Yohji Okada, Hiroaki Koyanayi, Kouichi Kakihara. New concept of miracle magnetic bearings. In *9th International Symposium on Magnetic Bearings*, August 2004.
- [10] Fang Jiancheng, Sun Jinji. New permanent magnet biased radial magnetic bearing in magnetic suspending flywheel application. *Journal of Beijing University of Aeronautics and Astronautics*, 32(11), 2006.
- [11] Huang Feng, Zhu Huangqiu, Xie Zhiyi, et al. Parameter Design and Analysis for Two-degrees of Freedom Radial Hybrid Magnetic Bearings. *China Mechanical Engineering*, 18(10), 2007.
- [12] Martin Reisinger, Wolfgang Amrhein, Siegfried Silber, et al. Development of a low cost permanent magnet biased bearing. In *9th International Symposium on Magnetic Bearings*, August 2004.
- [13] Kasarda M. E. F., Allaire P. E., Norris P. M. Experimentally determined rotor power losses in homopolar and heteropolar magnetic bearing. *Journal of Engineering for Gas Turbines and Power*, 121(4), 1999.